A Mn(II)−Mn(III) EPR Signal Arises from the Interaction of NO with the S_1 State of the Water-Oxidizing Complex of Photosystem II†

Josephine Sarrou, Nikolaos Ioannidis, Yannis Deligiannakis, and Vasili Petrouleas*

Institute of Materials Science, NCSR "Democritos", 15310 Aghia Paraskevi Attikis, Greece

Received November 18, 1997; Revised Manuscript Received January 20, 1998

ABSTRACT: It was shown recently [Goussias, C., Ioannidis, N., and Petrouleas, V. (1997) *Biochemistry 36*, 9261−9266] that incubation of photosystem II preparations with NO at −30 °C in the dark results in the formation of a new intermediate of the water-oxidizing complex. This is characterized by an EPR signal centered at $g = 2$ with prominent manganese hyperfine structure. We have examined the detailed structure of the signal using difference EPR spectroscopy. This is facilitated by the observations that NO can be completely removed without decrease or modification of the signal, and illumination at 0 °C eliminates the signal. The signal spans 1600 G and is characterized by sharp hyperfine structure. ^{14}NO and ^{15}NO cw EPR combined with pulsed ENDOR and ESEEM studies show no detectable contributions of the nitrogen nucleus to the spectrum. The spectrum bears similarities to the experimental spectrum of the Mn(II)−Mn(III) catalase [Zheng, M., Khangulov, S. V., Dismukes, G. C., and Barynin, V. V. (1994) *Inorg. Chem. 33*, 382−387]. Simulations allowing small variations in the catalase-tensor values result in an almost accurate reproduction of the NO-induced signal. This presents strong evidence for the assignment of the latter to a magnetically isolated Mn(II)−Mn(III) dimer. Since the starting oxidation states of Mn are higher than II, we deduce that NO acts effectively as a reductant, e.g., Mn(III)−Mn(III) + NO → Mn(II)−Mn(III) + NO^+. The temperature dependence of the nonsaturated EPR-signal intensity in the range 2−20 K indicates that the signal results from a ground state. The cw microwave power saturation data in the range 4−8 K can be interpreted assuming an Orbach relaxation mechanism with an excited state at $\Delta = 42$ K. Assuming antiferromagnetic coupling, $-2J\mathbf{S}_1\cdot\mathbf{S}_2$, between the two manganese ions, J is estimated to be 10 cm^{-1}. The finding that an EPR signal from the Mn cluster of PSII can be clearly assigned to a magnetically isolated Mn(II)−Mn(III) dimer bears important consequences in interpreting the structure of the Mn cluster. Although the signal is not currently assigned to a particular S state, it arises from a state lower than S_1, possibly lower than S_0, too.

Significant progress has been made recently in probing the lower S states of the water-oxidizing complex of photosystem II, PSII,[1] by EPR spectroscopy. The complex, thought to be a cluster of four manganese atoms, undergoes four one-electron oxidation state transitions, S_0-S_1, ..., S_3-S_4, during sequential absorption of photons by PSII (for reviews, see refs *1*−*5*). Of the various S states, S_2 is the most extensively studied one based on the characteristic multiline and alternative EPR signals (reviewed in ref *6*). It has been considerably more difficult to probe the lower S states. An integer spin EPR signal at $g = 4.8$ has been reported earlier for the S_1 state in parallel mode by Dexheimer and Klein (*7*), and this has been recently reproduced and further characterized by Yamauchi et al. (*8*). In another recent advance, Goussias et al. (*9*) have shown that incubation of PSII membranes in the S_1 state with NO at −30 °C results in the formation of a new intermediate originating from the Mn cluster. Its EPR spectrum, centered at $g = 2$, shows pronounced hyperfine structure with intense features in the high-field region of the spectrum. Although the signal can in principle be understood as being due to the interaction of the spin $^1/_2$ of the NO radical with the integer spin of the S_1 state, redox equilibria of NO with the S_1 state have been considered (*9*). The S_0 state, although a half-integer spin state, has escaped detection until very recently. Messinger et al. (*10*) reported an S_0* EPR multiline signal following chemical reduction with hydrazine to an S_{-1} state and subsequent illumination or following reduction with hydroxylamine. A similar signal has been reported by Åhrling et al. (*11*) to oscillate with period 4 in a flash sequence. The presence of 0.5−3% methanol is required for the observation of the signal, which consists of a large number of weak lines spaced over a spectral breadth of approximately 2400 G. These new signals, in combination with the signals from the higher S states, offer strong experimental tools to test earlier proposals concerning structure and valence state composition

† This work was supported by the EC Grants ERBCHRXCT940524, ERBFMBICT961440, and the PENED 1139 grant of the Greek General Secretariat of Research and Technology.

* Corresponding author: Inst. Mat. Sci., NCSR "Democritos", 15310 Aghia Paraskevi Attikis, Athens, Greece. Tel.: +301 650 3344. Fax: +301 6519430. E-mail: vpetr@ims.ariadne-t.gr.

[1] Abbreviations: PSII, photosystem II; BBY membranes, thylakoid membrane fragments enriched in PSII; S-states, S_0, ..., S_4 oxidation states of the water oxidising complex; tyr Y_Z, tyr Y_D, the fast and slow tyrosine electron donors of PSII; Q_A, Q_B, the primary, secondary plastoquinone electron acceptors of PSII; cw EPR, continuous wave electron paramagnetic resonance; MES, 2-[*N*-morpholineethanesulfonic acid]; chl, chlorophyll; ESEEM, electron spin−echo envelope modulation; ENDOR, electron nuclear double resonance.

S0006-2960(97)02828-6 CCC: $15.00
Published on Web 02/25/1998

and advance our understanding of the catalytic activity of this unique Mn complex.

In this report, we present a detailed characterization of the signal resulting from the interaction of the S_1 state with NO. Reliable representations of the signal over the full spectral region are obtained by a number of EPR difference techniques. Isotopic substitution studies, ^{15}NO for ^{14}NO, reveal no contribution of the nitrogen nucleus. Spectral simulations provide clear evidence for the assignment of the signal to a magnetically isolated Mn(II)−Mn(III) pair. Power and temperature dependence indicate antiferromagnetic coupling and a ground-state origin of the signal.

MATERIALS AND METHODS

PSII-enriched thylakoid membranes were isolated from market spinach by standard procedures (*12*, *13*). Samples for EPR measurements were suspended in 0.4 M sucrose, 15 mM NaCl, 5 mM $MgCl_2$, and 40 mM MES, pH 6.5, at 5−6 mg chl/mL (4 mm EPR tubes). The NO treatment was carried out anaerobically at 0 °C in the EPR tubes by slowly bubbling 4 mL of a mixture of NO and N_2 of $^2/_3$ v/v ratio, for 1 min. The samples were subsequently incubated at −30 °C overnight (*9*). ^{15}NO was synthesized from potassium nitrite (99% atom ^{15}N obtained from Isotec Inc.). Illumination of the samples was performed with a 340 W projection lamp filtered through a solution of $CuSO_4$.

Cw EPR measurements were obtained with a Bruker ER-200D-SRC spectrometer interfaced to a personal computer and equipped with an Oxford ESR 900 (above 4 K), or ESR 10 cryostat (between 2 and 4 K), an Anritsu MF76A frequency counter, and a Bruker 035M NMR gaussmeter. Temperature calibration was achieved with the use of an external thermocouple. Thermal gradients were within 0.2° between 4 and 10 K and within 0.5° above 10 K. Relatively large temperature uncertainties were observed with the ESR 10 cryostat. Accordingly, the free NO peak in the $g = 2$ region was used as an approximate internal standard for temperature calibration, assuming Curie variation in the range 2−4 K. In the study of the temperature dependence of the microwave power saturation, the likely influence of the modulation field amplitude on $P_{1/2}$ was examined. No significant dependence was observed in the range of 8−25 G_{pp} modulation amplitude.

Electron spin−echo experiments were carried with a Bruker ESP 380 spectrometer equipped with a cylindrical dielectric resonator, an ESP 360 DICE ENDOR system, and an ENI A500 rf amplifier. Electron spin−echo envelope modulation (ESEEM) data (*14*) were obtained by applying the three-pulse ($\pi/2$-τ-$\pi/2$-T-$\pi/2$-echo) sequence. The $\pi/2$ pulse had a 16 ns duration. Pulsed electron nuclear double resonance (ENDOR) spectra were recorded by applying the Mims and Davis sequences (*15* and references therein).

RESULTS

The isotopic substitution studies and the theoretical simulations presented in this paper require accurate measurements of the NO-induced multiline signal. Although the signal is stronger than the S_2 multiline (*9*), difference spectroscopy is required in order to distinguish clearly all features of the spectrum. Figure 1 shows difference spectra

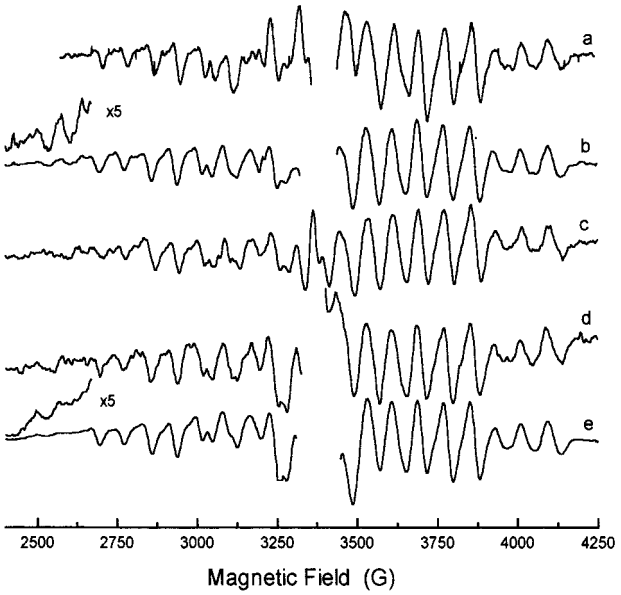

FIGURE 1: The NO-induced multiline signal in samples incubated initially with approximately 0.5−0.6 mM NO at −30 °C for longer than 12 h. Comparison of difference spectra obtained (see text for details): (a) after subtraction of the trace recorded following 5 min incubation at −5 °C (this eliminates reversibly the signal), (b) as in panel a but after prior removal of NO (c) as in panel b but in the presence of 1% v/v methanol, (d) after removal of NO and subtraction of the trace recorded following illumination at 0 °C, (e) after subtraction of the trace prior to the prolonged incubation at −30 °C. EPR conditions: $T = 11$ K (6 K in panel a); microwave frequency, 9.42 GHz; microwave power, 31 mW; modulation amplitude 25 G_{pp} (10 G_{pp} in panel a).

obtained by the methods described below. In all cases, the samples were incubated initially with approximately 0.6 mM NO at −30 °C for longer than 12 h in order to develop a large signal size. It should be noted that the amount of Mn^{2+} released during this or the treatments described below was negligible.

(a) It was noted earlier that the multiline signal is reversibly lost by a brief (1 min) warming up to 0 °C (*9*). The same behavior is observed during a few minutes of incubation at −5 °C. Background signals are not affected by this treatment. Figure 1a shows the difference spectrum resulting from the subtraction of the trace obtained after a brief incubation at −5 °C.

(b) The free NO peak at $g \leq 2$ interferes severely with the spectrum. We observed that the multiline signal after its development is unaffected by the removal of NO. This is accomplished by a few cycles of brief evacuation of the sample at 0−4 °C followed by flushing with N_2. During evacuation, the signal is lost reversibly due to the high temperature of the treatment. Incubation of the sample at −30° C for about 30 min restores the full size of the signal. Subtraction of the spectra from the last two treatments results in the spectrum shown in Figure 1b.

(c) The spectrum in Figure 1c was obtained in a similar way with spectrum 1b, but methanol at 1% v/v was present during the NO treatment. It was observed that methanol, which is essential for the appearance of the S_0* signal (*10*, *11*), decreases the size of the present signal but does not seem to affect the signal shape.

(d) Figure 1d is a dark minus light difference spectrum. A sample prepared as in spectrum b (dark) was illuminated

at 0 °C for 1 min (in the absence of exogenous electron acceptors) and subsequently kept in darkness for 30 min at −30 °C (light). Illumination eliminates the signal due to advancement to higher S states (the photochemical activity of the samples following the NO treatment will be examined in a forthcoming report), while the dark incubation at −30 °C serves both, to confirm elimination of the signal and to depopulate higher S states (e.g., S_2) that could potentially contribute to the background spectrum. The central part of the spectrum containing a contribution from the light-induced increase in signal II was removed. The latter signal was recovered after removal of NO since irreversible reactions leading to the formation of an iminoxyl radical (*16*) proceed very slowly at −30 °C (*9*).

(e) The spectrum of a sample incubated with NO for 30 h at −30 °C is also shown, Figure 1e, after subtraction of the spectrum during the first minute of incubation with NO. Although the central part of the spectrum containing contributions from the free NO signal (this signal decreases during the prolonged incubation) has been removed, the outer part exhibits a very good signal-to-noise ratio and was included for comparison.

Examination of the spectra in Figure 1 shows that the main features are reproduced in the various preparations. Small differences are observed in the individual peaks (beyond the obvious ones mentioned above), and these should be kept in mind when estimating (see below) the likely changes during isotopic substitution or the differences from the theoretical simulation. General characteristics of the signal are the following. The NO-induced multiline signal has sharp features and lies on a flat background. The high-field limit of the spectrum is well-defined ending at 4100 G. The low-field lines are weaker, but close examination indicates that the signal ends at 2500 G. The overall width of the signal is accordingly 1600 G.

Isotopic Replacement of ^{14}NO with ^{15}NO. On the basis of the well-known affinity of NO for metal centers it was suggested in the earlier study that NO binds to the Mn cluster. The multiline signal could accordingly be the result of spin coupling of the unpaired electron of NO with the Mn cluster or could result from Mn oxidation or reduction due to internal charge transfer. The presence of NO or derivatives of it as ligands to the Mn cluster should in principle be detectable by ^{14}NO and ^{15}NO substitution studies. Although cw EPR studies of the S_2-multiline signal have failed to detect nitrogen superhyperfine couplings (*17*−*19*), the presence of considerable electron spin density on NO should produce a detectable isotopic effect. Weak couplings on the other hand should be detectable by ENDOR or ESEEM spectroscopies.

Samples treated with ^{14}NO and ^{15}NO were measured with cw EPR at different temperatures, modulation amplitudes, and microwave power values. The differences among the isotopically substituted samples were in all cases very small. Two sets of spectra are shown in Figure 2. In the upper set, difference spectra were obtained as in Figure 1a. In the lower set, NO was removed prior to the EPR measurements as in Figure 1b. Apart from the central region, which suffers from subtraction artifacts and has been removed, the differences in the individual peaks are within the variations observed in the spectra from different preparations, Figure 1. As a control of the isotopic enrichment, samples prepared so as to develop a large iminoxyl radical, from the interaction of

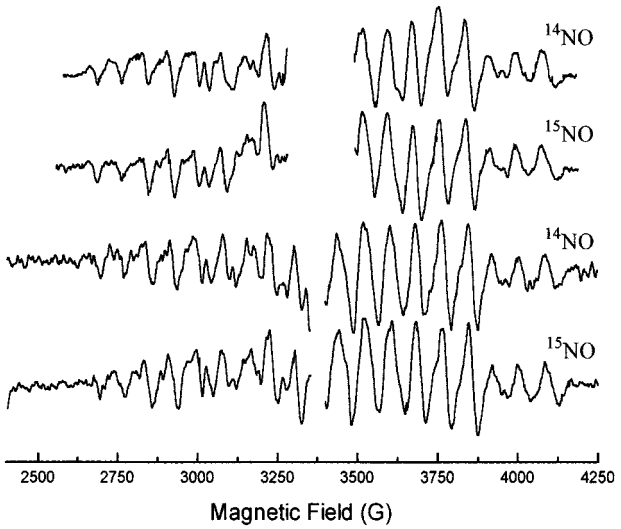

FIGURE 2: Comparison of the NO-induced multiline signals obtained with ^{14}NO and ^{15}NO. The upper set of the difference spectra was obtained as in Figure 1a, while the lower set was recorded after removal of NO as in Figure 1b. EPR conditions: T = 6 K; microwave frequency, 9.42 GHz, microwave power 126 mW (upper set of spectra) or 31 (lower set of spectra) and modulation amplitude 5 G_{pp}.

NO with Tyr $Y_D^{\bullet}$, showed a very pronounced (approximately 100%) isotopic effect (data not shown).

In the absence of strong couplings, a search for weaker interactions was made by ENDOR and ESEEM spectroscopies. Typically, hyperfine couplings up to a few tens of Gauss are better resolved by ENDOR (*20*), while couplings of a few Gauss can be resolved by ESEEM (*14* and references therein). The pulsed-ENDOR spectra of the Mn recorded across the multiline signal showed (data not shown) no evidence of nitrogen couplings in either the ^{14}NO- or the ^{15}NO-treated sample. In the ESEEM spectra, a peak at the nuclear Larmor frequency of the ^{15}N nucleus (1.5 MHz at 3500 G), which is absent in the ^{14}NO samples (data not shown), is the only difference resolved. This peak is attributed to distant ^{15}N nuclei from ^{15}NO weakly interacting with the spin of the manganese cluster.

The simplest interpretation of the absence of a detectable isotopic effect, consistent with the earlier observations (*9*) and the data to be presented below (see also the Discussion), is that NO binds slowly to the S_1 state and transfers its unpaired electron to a Mn ion, $Mn^n + NO \rightarrow Mn^{n-1} + NO^+$. NO^+ in turn diffuses away.

Theoretical Simulations Indicate a Mn(II)−*Mn(III) Dimer*. The apparent similarity in the splitting of the hyperfine lines between the present and the S_2 multiline (*9*) prompted us to carry out simulations assuming a Mn configuration similar to the one giving rise to the S_2 multiline. This would correspond to the case of NO acting as an oxidant (a very unlikely possibility; *9*) or, approximately, to the case of strong antiferromagnetic coupling of NO with one of the Mn ions, (*9*) (a possibility not supported by the isotopic substitution experiments above). We accordingly did rather extensive simulations employing the approach of Zheng and Dismukes (*6*) and assuming alternative configurations, 3Mn(III)−1Mn(IV) or 1Mn(III)−3Mn(IV). In all cases, the deviations were significant.

In searching over the literature, an interesting similarity was observed with the spectrum of the Mn(II)−Mn(III)

Table 1: Comparison of the Hyperfine and Zero-Field-Splitting Parameters of the NO-Induced Multiline Signal in PSII, with Those from the Simulation of the Mn(II)−Mn(III) Catalase (*22*)

a. Hyperfine, *A*(MHz), **g** Tensor Values, and Residuals (Sum of Squared Deviations in Amplitude Divided by the Sum of Squared Amplitudes of the Data Points), *R*, of the Least-Squares Fitting

	Mn(II) (A_x, A_y, A_z) A_{iso}	Mn(III) (A_x, A_y, A_z) A_{iso}	(g_x, g_y, g_z) g_{iso}	*R* %
PSII (NO induced)	(−553, −553, −765) −625	(228, 228, 208) 220	(1.970, 1.970, 2.011) 1.983	1.6
Mn(II,III) cat	(−529, −502, −730) −587	(222, 210, 236) 223	(1.958, 1.965, 2.025) 1.983	3.6

b. Calculated Intrinsic Hyperfine *a*(MHz) and Zero-Field-Splitting Parameters, as in ref *22*

		Mn(III)		
	Mn(II) a_{iso}	($a_{x,y}$, a_z) a_{iso}	*D*/*J*	*D* (cm^{-1})
PSII (NO induced)	−267	(−214, −111) −180	0.43	−4.3
Mn(II,III) cat	−253	(−207, −124) −179	0.47	<0

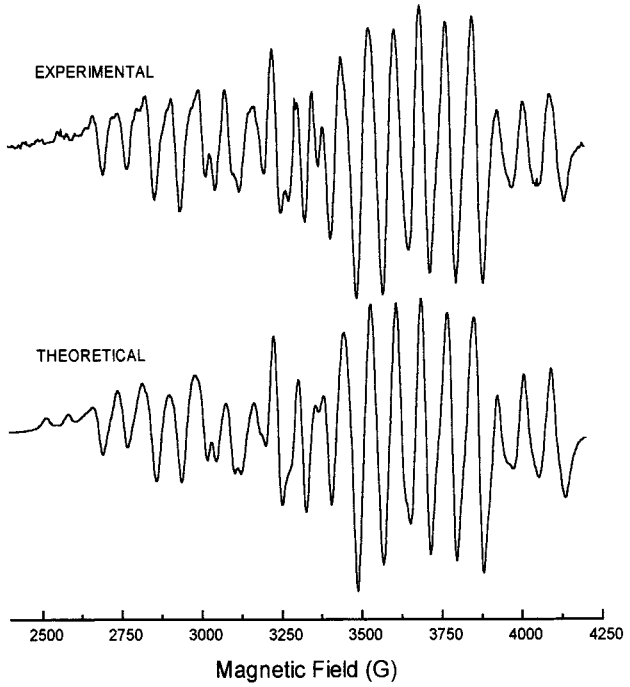

FIGURE 3: Theoretical simulation of the NO-induced spectrum assuming an $S = {}^1/_2$ state of a Mn(II)−Mn(III) dimer and the parameter values of Table 1. The experimental spectrum was obtained by incubation with ca. 0.6 mM NO at −30 °C for 36 h followed by removal of NO. The baseline for subtraction was obtained by a 10 min incubation at −5 °C. EPR conditions as in Figure 1.

catalase from *Thermus thermophilus* (*21*, *22*). We accordingly performed theoretical simulations assuming a Mn(II)−Mn(III) dimer and using as starting parameters those that simulate accurately the catalase spectrum. To reduce the number of parameters, we assumed axial symmetry. A broad search was made in the parameter space before a least-squares procedure was applied. The parameters converged to the values listed in Table 1a. The resulting theoretical spectrum is compared with the experimental one in Figure 3. The agreement is very good and strongly supports the assignment of the present signal to a Mn(II)−Mn(III) dimer.

The simulation parameters in Table 1a were used to calculate the intrinsic hyperfine and zero-field-splitting parameters by following the same approach as in ref *22*. The results are listed in Table 1b. Included is also an estimate of *D* based on the calculated value of *D*/*J* and the approximate value of *J* from the analysis in the next section.

Microwave-Power and Temperature Dependence of the Signal. The continuous wave power saturation studies of the NO-induced multiline signal, at various temperatures, are illustrated in Figure 4. The data are fitted with the function $I = CP^{1/2}/(1 + P/P_{1/2})^{0.5b}$, where *I* is the amplitude of the EPR signal, *C* depends on the apparatus and the concentration of the spins, *P* is the microwave power in mW, $P_{1/2}$ is the power for half-saturation, and *b* is the inhomogeneity parameter (*23*, *24*). In all cases, the fitting procedure gave a value of approximately 1 for *b*. The latter result and the observation that the power saturation data are independent of the modulation-amplitude range of values (see Materials and Methods) imply that the $P_{1/2}$ values are approximately proportional to the spin−lattice relaxation rate, $1/T_1$ (*24*).

The temperature variation of the spin−lattice relaxation rate above 2 K is usually attributed to either of two relaxation mechanisms, an Orbach (spin−lattice relaxation through an excited state at energy Δ above the ground state) or a Raman (relaxation through a virtual excited state) process (*25*). It should be possible in principle to distinguish between the two mechanisms, based on the different temperature dependence of the relaxation rate, $1/T_1 \propto \exp(-\Delta/kT)$ for an Orbach process, $1/T_1 \propto T^n$, $3 \leq n \leq 9$, for a Raman process. This requires, however, very accurate relative temperature determination (small $\Delta T/T$), which is not easy in low-temperature EPR spectroscopy. We have assumed, as was done in similar studies of the S_2 multiline (*26*−*28*, see also *24*), that in the temperature range of interest, 2−8 K, the Orbach process dominates. Figure 4 (inset) shows the plot of ln $P_{1/2}$ versus $1/T$ (assuming an Orbach process) in the temperature range 2−8 K. The negative slope of the linear fit is equal to $\Delta = 26$ K (19 cm^{-1}). A similar analysis in a more restricted temperature range, 4−8 K, results in a larger energy separation, $\Delta = 42$ K (29 cm^{-1}). Alternatively, an analysis assuming a Raman process (not shown) gives $n = 7$, i.e., $P_{1/2} \propto T^7$, and $n = 8$ in the two respective temperature ranges. The variation in the fitting parameters may be due to the larger relative temperature uncertainties (see Materials

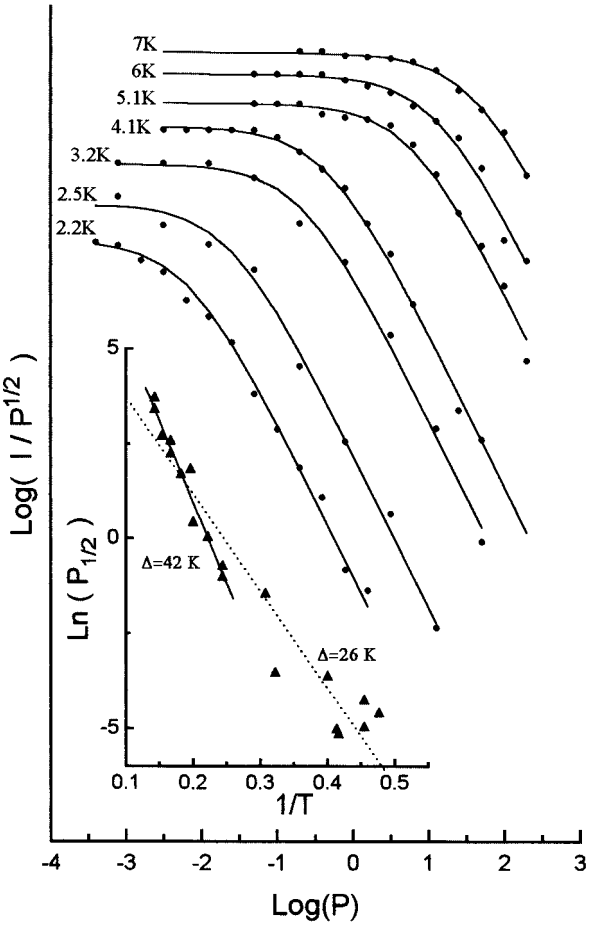

FIGURE 4: Representative microwave power saturation data in the temperature range 2−8 K. Continuous traces are computer fits as described in the text. (Inset) Fitting of the $P_{1/2}$ values assuming an Orbach process in an extended temperature range (dotted trace) and in the restricted range 4−8 K (continuous trace).

and Methods) or to the contribution of additional relaxation mechanisms, below 4 K. Accordingly, the estimate $\Delta \approx 40$ K is probably more reliable. This is within the range of energy separations expected for a Mn(II)−Mn(III) antiferromagnetically coupled dimer. In the case of the S_2 multiline, the estimate of Δ is somewhat higher, 30 (*26*) or 36.5 (*28*) cm^{-1}. Of course no direct comparison can be made since the latter signal results presumably from 4 interacting Mn ions at high oxidation states.

The temperature dependence of the nonsaturated-signal intensity is depicted in Figure 5 as the plot of $1/I$ vs T. It is apparent that the EPR intensity follows Curie law behavior ($1/I \propto T$) at low temperatures, implying that the state giving rise to the signal is a ground state, or at least it does not lie higher than ca. 2 K above the ground state. The plot shows an increasing upward curvature at temperatures above about 9 K. This can be due to thermal population of higher states and/or relaxation broadening of the lines. The fact that relaxation broadening dominates at higher temperatures is suggested by the practically zeroing of the signal intensity at ca. 21 K and above. With two antiferromagnetically interacting spins $S_1 = {}^5/_2$ [Mn(II)] and $S_2 = 2$ [Mn(III)], $-2J\mathbf{S}_1\cdot\mathbf{S}_2$, the first excited state (spin quartet) lies at an energy $\Delta = -3J$ and the next higher state (spin sextet) at $-8J = (8/3)\Delta$ above the ground doublet state. Initial simulations with variable Δ values (not shown) indicate that

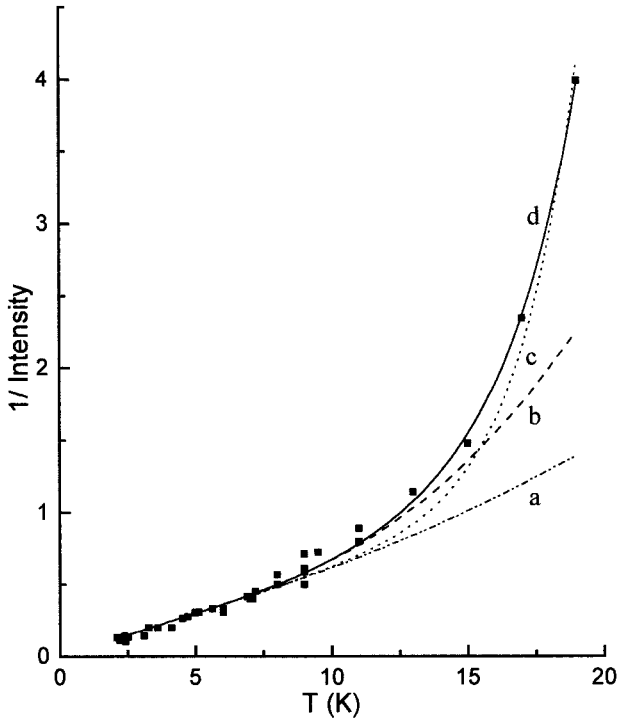

FIGURE 5: Reciprocal spectral intensity vs temperature plot under nonsaturating conditions. Simulation curves are calculated assuming thermal population of an excited spin quartet at 42 K (a), plus additional intensity loss due to an Orbach (b), or Raman (c), or both relaxation mechanisms (d).

the data above 15 K cannot be simulated assuming simple Boltzmann statistics. It is difficult to estimate, however, at what temperature broadening dominates the temperature variation, but the data can be used to set a lower limit to Δ of approximately 20 K, which is compatible with the higher value of Δ obtained by the Orbach analysis. To visualize qualitatively the effect of the various factors that result in the signal-intensity drop, we have constructed in Figure 5 theoretical curves assuming that the Boltzmann variation in the signal intensity is further modulated by the factor $1/(1 + \delta W_{rel})$, were δW_{rel} is the relative broadening of the lines due to relaxation. This follows from the approximate assumption that the product intensity × width of the lines at a given temperature remains constant regardless of the relaxation mechanism. δW_{rel} in turn is assumed to be proportional to $1/T_1$, which for an Orbach process varies as $\exp(-\Delta/kT)$ and for a Raman process as T^n, as was discussed above. Trace a in Figure 5 is accordingly calculated assuming simple Boltzmann temperature variation with $\Delta = 42$ K, trace b assuming in addition broadening due to an Orbach relaxation mechanism, trace c assuming modulation of the Boltzmann variation by a Raman mechanism, $n = 8$, and trace d assuming modulation by both relaxation mechanisms. Apparently, the Raman mechanism dominates at temperatures above 15 K, but the data below 15 K can be simulated assuming a small contribution from the Orbach relaxation mechanism (inducing a line broadening above ca. 9 K) in addition to the Boltzmann variation.

DISCUSSION

A consistent picture, which arises from the previous analysis is the following. There is no detectable contribution of NO to the NO-induced-multiline signal, and the signal

can be reproduced theoretically assuming a Mn(II) ($S = {}^5/_2$)−Mn(III) ($S = 2$) antiferromagnetically coupled dimer. The state producing the signal is a ground spin doublet. The first excited spin quartet lies at about $\Delta = 42$ K (29 cm^{-1}). The exchange coupling of the two spins, $-2J\mathbf{S}_1\cdot\mathbf{S}_2$, is estimated accordingly $J = -\Delta/3 \approx -10$ cm^{-1}, which is reasonable for a Mn(II)−Mn(III) dimer. The hyperfine and zero-field-splitting parameters of the individual ions are listed in Table 1.

A comparison of the Mn parameters in the present and the Mn-catalase case in Table 1b, indicates a general similarity in the two systems. The most notable difference is in the hyperfine anisotropy of the Mn(III), which appears to be enhanced in PSII, compared to the catalase or the model complexes examined in (*22*). This could indicate a lower symmetry environment in the PSII Mn(III), e.g. as a result of constraints imposed by the bonding to the second pair of the Mn atoms. It should be noted, however, that the calculation of the hyperfine values in Table 1b has assumed that the intrinsic anisotropy of the Mn(II) is negligible (*22*) and the observed anisotropy in the *A* Mn(II) values is totally due to admixing with the $S = {}^3/_2$ excited state, which bears the projected anisotropy of the Mn(III) (*22*). Regardless of the particular theoretical model, the fact that the two experimental spectra can be almost accurately simulated by small variations in the same set of parameters is strong evidence for the same nuclearity and oxidation state composition. It is not obvious at present how far the similarity can be extended to the microenvironment of the Mn ions. The three-dimensional structure of the di-Mn catalase from *Thermus thermophilus* has been recently resolved to high resolution in the fully reduced [Mn(II)−Mn(II)] and the oxidized state [Mn(III)−Mn(III)] (*29*). The Mn−Mn distance is 3.18 Å in the reduced and 3.14 Å in the oxidized state. Two exogenous ligands, modeled as hydroxide (or oxygen in the oxidized form) and water, as well as a glutamate, bridge the two metal ions. This structure bears analogies to the Mn pair at 3.3 Å in the proposed structure of the Mn cluster based on EXAFS studies (*4*). Simple considerations on the other hand would place the pair producing the present signal to a terminal position so as to minimize magnetic coupling with the rest of the complex. The structural implications of the present results will hopefully be clarified in future studies.

All signals associated with the Mn complex, that have been reported so far, result from known S-states (natural or modified). The redox composition or even the nuclearity (number of Mn ions contributing to the signal) in probably all cases has, however, been controversial. The two likely redox assignments of the S_1 state are [2Mn(III)−2Mn(IV)] (*30*, *4*) or [4Mn(III)] (*31*, *6*). The present signal is well characterized spectroscopically as a Mn(II)−Mn(III) dimer, but the assignment to a particular S state is not obvious. According to the above redox state assignments, the signal must result from a state lower than S_1. It was shown earlier that NO destabilizes rapidly the S_2 state (*9*). The present analysis implies that the reduction proceeds even further, albeit at a much lower rate. NO probably interacts with the Mn cluster by one-electron reduction of Mn(IV) or Mn(III) releasing NO^+. As no isotopic effect due to the nitrogen nucleus can be detected, NO^+ must diffuse away (probably to the aqueous phase). Strictly speaking, it cannot be excluded that NO or its derivatives may be bound on the EPR silent part of the Mn cluster. It is of note, however, that, after the evolution of the signal, NO can be completely removed without any modifications of the signal shape or reduction of the signal size, Figure 1. On the contrary, we have routinely observed that removal of NO eliminates the $g = 4$ signal (data not shown) originating from the binding of NO to the acceptor side nonheme Fe(II) (*32*). The present signal has fewer hyperfine lines and reduced spectral breadth compared to the recently reported signal from the S_0* state detectable only in the presence of methanol (*10*, *11*). The presence of methanol does not modify the NO-induced signal, Figure 1c, except that it decreases its size. It is possible then that the present signal results from a state lower than S_0, although the possibility that the two signals result from different isoelectronic configurations of S_0 cannot be ruled out. Given the much larger spectral breadth of the S_0* signal and the fact that the present signal is attributed to a Mn(II)−Mn(III) dimer, it is likely that the S_0* signal results from a magnetic tetramer.

ACKNOWLEDGMENT

Many thanks are due to Dr. Ch. Goussias for help in the initial stages of this work and Drs. M. Zheng and G. C. Dismukes for generously providing their EPR simulation program (*6*), Dr. G. Schansker for helpful suggestions, and Mr. A. Tsohos for help with the computer fitting.

REFERENCES

1. Rutherford, A. W. (1989) *Trends Biol. Sci. 14*, 227−232.
2. Hansson, Ö., and Wydrzynski, T. (1990) *Photosynth. Res. 23*, 131.
3. Debus, R. J. (1992) *Biochim. Biophys. Acta 1102*, 269−352.
4. Yachandra, V. K., Sauer, K., and Klein, M. P. (1996) *Chem. Rev. 96*, 2927−2950.
5. Britt, R. D. (1996) *Advances in Photosynthesis: Vol. 4 Oxygenic Photosynthesis: The Light Reactions* (Ort, R. D., and Yocum, C. F., Eds.) pp 137−164, Kluwer Academic Publishers, Dordrecht, The Netherlands.
6. Zheng, M., and Dismukes, G. C. (1996) *Inorg. Chem. 35*, 3307−3319.
7. Dexheimer, S. L., and Klein, M. P. (1992) *J. Am. Chem. Soc. 114*, 2821−2826.
8. Yamauchi, T., Mino, H., Matsukawa, T., Kawamori, A., and Ono, T. (1997) *Biochemistry 36*, 7520−7526.
9. Goussias, C., Ioannidis, N., and Petrouleas, V. (1997) *Biochemistry 36*, 9261−9266.
10. Messinger, J., Nugent, J. H. A., and Evans, M. C. W. (1997) *Biochemistry 36*, 11055−11060.
11. Åhrling, K. A., Peterson, S., and Styring, S. (1997) *Biochemistry 36*, 13148−13152.
12. Berthold, D. A., Babcock, G. T., and Yocum, C. F. (1981) *FEBS Lett. 134*, 231−234.
13. Ford R. C., and Evans, M. C. W. (1983) *FEBS Lett. 160*, 159−164.
14. Dikanov, S. A. and Tsvetkov, Y. D. (1993) *Electron Spin−Echo Envelope Modulation (ESEEM)*, CRC Publishers, Boca Raton, FL.
15. Gemberle, C., and Schweiger, A. (1991) *Chem. Rev. 91*, 1481.
16. Sanakis, Y., Goussias, Ch., Mason, R. P., and Petrouleas, V. (1996) *Biochemistry 36*, 1411−1417.
17. Andreasson, L.-E. (1989) *Biochim. Biophys. Acta 973*, 465−467.
18. Beck, W. F., de Paula, J. C., and Brudvig, G. W. (1986) *J. Am. Chem. Soc. 108*, 4018−4022.
19. Britt, R. D., Zimmermann, J.-L., Sauer, K., and Klein, M. P. (1989) *J. Am. Chem. Soc. 111*, 3522−3532.

20. Hoffman, B. M., DeRose, V. J., Doan P. E., Gubriel, R. J., Houseman, A. L. P., and Telser, J. (1993) *Biological Magnetic Resonance* (Berliner, L. J., and Reuben, L., Eds.) pp 151−218, Plenum Press, New York.
21. Khangulov, S. V., Barynin, V. V., Voevodskaya, N. V., and Grebenko, A. I. (1990) *Biochim. Biophys. Acta 1020*, 305−310.
22. Zheng, M., Khangulov, S. V., Dismukes, G. C., and Barynin, V. V. (1994) *Inorg. Chem. 33*, 382−387.
23. Rupp, H., Rao, K. K., Hall, D. O., and Cammack, R. (1978) *Biochim. Biophys. Acta 537*, 255−269.
24. Yim, M. B., Kuo, L. C., and Makinen, M. W. (1982) *J. Magn. Reson. 46*, 247−256.
25. Abragam, A., and Bleaney, B. (1970) *Electron Paramagnetic Resonance of Transition Ions*, Clarendon, Oxford, England.
26. Hansson, Ö., Andréasson, L.-E., and Vänngård, T. (1984) in *Advances in Photosynthesis Research* (Sybesma, C., Ed.) Vol. I, pp 307−310, Nijhoff and Junk, The Hague, The Netherlands.
27. de Paula, J. C., and Brudvig, G. W. (1985) *J. Am. Chem. Soc. 107*, 2643−2648.
28. Lorigan, G. A., and Britt, R. D. (1994) *Biochemistry 33*, 12072−12076.
29. Barynin, V. V., Hempstead, P. D., Vagin, A. A., Antonyuk, S. V., Melik-Adamyan, W. R., Lamzin, V. S., Harrison, P. M., and Artymiuk, P. J. (1997) *J. Inorg. Biochem. 67 (1−4)*, Abstracts of ICBIC-8, 196.
30. Riggs, P. J., Mei, R., Yocum, C. F., and Penner-Hahn, J. E. (1992) *J. Am. Chem. Soc. 114*, 10650−10651.
31. Kusunoki, M., Ono, T. A., Matsushita, T., Oyanagi, H., Inoue, Y. J. (1990) *Biochem. 108*, 560−567.
32. Petrouleas, V., and Diner, B. A. (1990) *Biochim. Biophys. Acta 1015*, 131−140.

BI972828C